

# Dynamic Majorana resonances and universal symmetry of nonequilibrium thermoelectric quantum noise

Sergey Smirnov

*P. N. Lebedev Physical Institute of the Russian Academy of Sciences, 119991 Moscow, Russia\**

(Dated: December 13, 2019)

Nonequilibrium states of a nanoscopic system may be achieved by both applying a bias voltage  $V$  to its contacts and producing a difference  $\Delta T$  in their temperatures. Then the total current results from two competing flows, induced by  $V$  and  $\Delta T$ , respectively. Here we explore finite frequency quantum noise of this thermoelectric current flowing through a quantum dot whose low-energy dynamics is governed by Majorana degrees of freedom. We demonstrate that at finite frequency  $\omega$  Majorana zero modes induce a perfect universal symmetry between photon emission and absorption spectra and produce universal thermoelectric resonances in their frequency dependence in contrast to non-Majorana quantum noise which is either asymmetric or non-universal. In particular, at low temperatures the differential thermoelectric quantum noise induced by Majorana zero modes shows resonances with a nontrivial maximum  $\frac{e^3}{h} \log(2^{1/4})$  at  $\omega = \mp \frac{|eV|}{h}$  when  $k_B \Delta T \ll |eV|$ . Our results challenge cutting-edge experiments using quantum noise detectors to reveal the universal spectral symmetry and resonant structure of the Majorana thermoelectric finite frequency quantum noise.

## I. INTRODUCTION

Quantum materials possessing various topological superconducting phases admit, among others, specific phases characterized by the presence of Majorana zero modes (MZMs). In such phases, achieved via quantum phase transitions, some pairs of Majorana fermions break during a quantum phase transition and form MZMs localized at interfaces separating topologically different systems. While in the particle physics Majorana fermions [1] are Abelian, their condensed matter implementation assumes non-Abelian nature of MZMs which are highly nonlocal quasiparticles. In particular, MZMs appear at the opposite ends of one-dimensional systems effectively implementing [2–6] the topological superconducting phase of the Kitaev model [7] using topological insulators [8, 9] or spin-orbit coupled semiconductors [10, 11].

Experiments [12–14] on detections of Majorana signatures usually analyze quantum transport through a mesoscopic system, more specifically the mean electric current providing the differential conductance. On one side, such transport experiments, although of high quality, might be opposed to experiments based on braiding MZMs for fully conclusive claims whether MZMs are present in a given system. On the other side, recent success in thermodynamic and transport experiments [15, 16] measuring the entropy of a mesoscopic system is very appealing for future experimental detection (see, *e.g.*, Ref. [17]) of Majorana tunneling entropy [18] to avoid any braiding and at the same time to unambiguously reveal MZMs in mesoscopic setups.

Braidings are, however, necessary for practical applications of MZMs in devices implementing topological quantum computations [19]. The final result of a sequence

of braid operations depends only on its topology. It is thus robust against many perturbations which have a local character and in this way implements fault-tolerant quantum computation protected from major sources of decoherence via global topologically nontrivial properties [20]. Remaining sources of decoherence include noise which is unavoidable in practical realizations of Majorana braiding influenced by an external environment of a realistic device [21].

In turn, in mesoscopic setups MZMs determine not only the mean values but also lead to significant noise of physical observables, such as the electric current, both in the static limit [22–26], and at finite frequencies [27–29]. Measuring noise of nonequilibrium electric currents provides at finite frequencies  $\omega$  photon emission ( $\omega < 0$ ) and absorption ( $\omega > 0$ ) spectra. These spectra, as shown below, are either asymmetric, when the Majoranas strongly overlap and form partially separated Andreev bound states, or symmetric but not universal, when the Majoranas are absent at all as in trivial quantum dot (QD) systems. The degree of this *spectral asymmetry* or *non-universality* is relatively easy to verify in contemporary experiments via dependence of the spectra on the gate voltage controlling the chemical potential.

In this paper we demonstrate that the above picture, which would commonly be observed for partially separated Andreev bound states or trivial systems, changes drastically when MZMs are involved in the competition between two nonequilibrium quasiparticle flows, excited, respectively, by a bias voltage  $V$  and a temperature difference  $\Delta T$ . Remarkably, the quasiparticle fluctuations, resulting in finite frequency quantum noise of the induced thermoelectric current, are shown to acquire *universal spectral symmetry* and *nontrivial resonant structure*.

Specifically, we present results for thermoelectric transport through a QD whose states are entangled with a Kitaev's chain in its topological superconducting phase supporting two MZMs at its ends as shown in Fig. 1. The QD also interacts with two normal metals, left

\* 1) sergej.physik@gmail.com

2) sergey.smirnov@physik.uni-regensburg.de

3) ssmirnov@sci.lebedev.ru

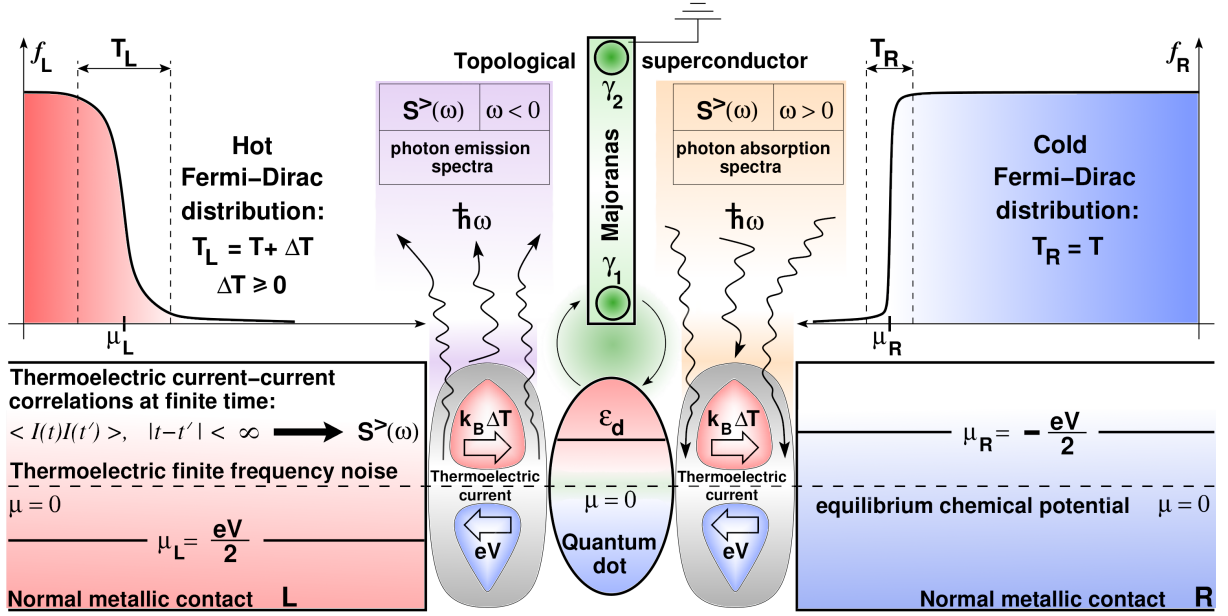


FIG. 1. A sketch of a realistic QD device where both a bias voltage  $V$  and a temperature difference  $\Delta T$  are the sources of nonequilibrium states of a QD. The QD is coupled via tunneling to two massive normal metals, the left ( $L$ ) and right ( $R$ ) contacts. The gray areas between the QD and contacts specify the nonequilibrium thermoelectric current incorporating two competing flows (big right-to-left and left-to-right arrows), excited, respectively, by  $V$  (the blue droplet) and by  $\Delta T$  (the red droplet). The device includes a topological superconductor (TS) with two MZMs  $\gamma_{1,2}$  at its ends (two green circles). The quasiparticle flows, denoted by the two thin vertical arc arrows around the green area, entangle the QD states with the Majoranas via tunneling processes involving  $\gamma_1$ .

and right contacts, whose chemical potentials and temperatures are denoted, respectively, as  $\mu_{L,R}$  and  $T_{L,R}$ ,  $\mu_L = -\mu_R = eV/2$  ( $eV < 0$ ),  $T_L = T + \Delta T$  ( $\Delta T \geq 0$ ),  $T_R = T$ , *i.e.* the left (right) contact is hot (cold). Instead of the temperature difference it is convenient to use the thermal voltage  $eV_T \equiv k_B \Delta T$ .

While the static ( $\omega = 0$ ) limit [30] of Majorana thermoelectric noise provides fluctuation physics at long times, it does not have access to the corresponding photon emission and absorption spectra which are of direct experimental interest in the quantum limit [31]. In contrast, at finite frequencies quantum fluctuations  $\delta I(t)$  of the thermoelectric current  $I(t)$  keep inside wealth of information about the photon spectra never explored in thermoelectric Majorana setups.

Here, for the case of the setup in Fig. 1, we explore the properties of these Majorana finite frequency thermoelectric quantum fluctuations encoded in the photon absorption and emission spectra obtained via the Fourier transform,  $S^>(\omega, V, V_T)$ , of the greater noise correlation function in the left contact,  $S^>(t - t', V, V_T) = \langle \delta I_L(t) \delta I_L(t') \rangle$ . To focus on universal properties we compute the differential thermoelectric finite frequency quantum noise,  $\partial S^>(\omega, V, V_T) / \partial V_T$ , which has universal units of  $e^3/h$ . In particular, when the MZMs are involved in the low temperature interplay between the two quasiparticle flows induced by, respectively,  $V$  and  $V_T$ , we predict (1) that the differential thermoelectric quantum noise (DTQN) acquires universal symmetry,

$\partial S^>(-\omega, V, V_T) / \partial V_T = \partial S^>(\omega, V, V_T) / \partial V_T$ ; (2) in the regime  $eV_T \gg |eV|$  it has a resonance located around  $\omega = 0$  with a nontrivial universal maximum  $[1 + \log(2)](e^3/h)$  reached exactly at  $\omega = 0$ ; (3) in the regime  $eV_T \ll |eV|$  the resonance located around  $\omega = 0$  persists but its maximum lowers down to another nontrivial universal maximum  $[1 + \log(2^{1/2})](e^3/h)$  also reached exactly at  $\omega = 0$ ; (4) in the same regime DTQN exhibits resonances located around  $\omega = \mp |eV|/\hbar$  with one more nontrivial universal maximum  $[\log(2^{1/4})](e^3/h)$  reached exactly at  $\omega = \mp |eV|/\hbar$ .

The paper is organized as follows. In Section II we discuss in detail the theoretical model involving MZMs and define the specific observable we explore, that is the thermoelectric quantum noise. The results are presented and thoroughly analyzed in Section III where the emphasis is made on universal behavior of the thermoelectric quantum noise. With Section IV we provide realistic parameters in the SI units and conclude that the universal results from Section III are well achievable in modern labs.

## II. THEORETICAL MODEL AND THERMOELECTRIC QUANTUM NOISE

To explore the essential aspects of quantum thermoelectric transport we describe the setup shown in Fig. 1 within a theoretical model specified by the Hamiltonians

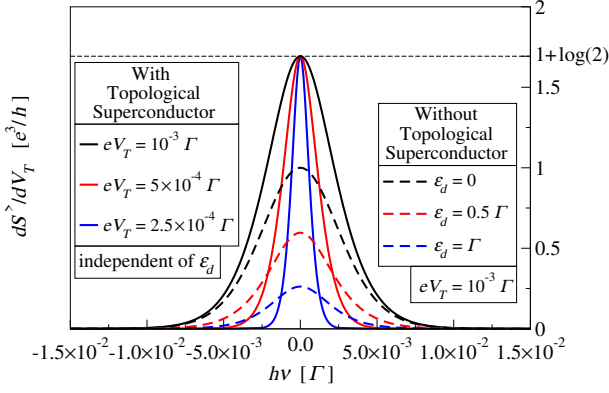


FIG. 2. DTQN  $\partial S^>(\nu, V, V_T)/\partial V_T$  as a function of the frequency  $\nu$  ( $h\nu = \hbar\omega$ ) is shown in the regime  $eV_T \gg |eV|$ . Here  $k_B T/\Gamma = 10^{-10}$ ,  $|\eta|/\Gamma = 10^3$ ,  $\xi/\Gamma = 10^{-4}$  and  $|eV|/\Gamma = 10^{-5}$ . The three solid curves demonstrate a resonance of  $\partial S^>(\nu, V, V_T)/\partial V_T$  located around  $\nu = 0$  for three different values of  $eV_T$ . The three dashed curves show the spectra of the trivial QD system,  $\xi = 0$ ,  $\eta = 0$ , for three different values of the gate voltage.

of the QD, contacts, TS, the Hamiltonians for the tunneling between the QD and contacts and for the tunneling between the QD and TS.

The QD has one nondegenerate single-particle level  $\epsilon_d$ . A gate voltage may tune the position of  $\epsilon_d$  with reference to the chemical potential  $\mu$ . The corresponding noninteracting Hamiltonian is  $\hat{H}_d = \epsilon_d d^\dagger d$ .

The normal metallic contacts are assumed to be noninteracting and large enough so that their energy spectra are continuous,  $\hat{H}_c = \sum_{l=L,R} \sum_k \epsilon_k c_{lk}^\dagger c_{lk}$ . Within energy ranges relevant for transport one traditionally assumes a constant density of states  $\nu_c/2$ . The contacts are in equilibrium with the corresponding Fermi-Dirac distributions,  $f_{L,R}(\epsilon) = \{\exp[(\epsilon - \mu_{L,R})/T_{L,R}] + 1\}^{-1}$ .

At low energies one may effectively capture relevant physics of the TS via the Hamiltonian  $\hat{H}_{tsc} = i\xi\gamma_2\gamma_1/2$  represented in terms of the Majorana operators  $\gamma_{1,2}$  satisfying the conjugation relation  $\gamma_{1,2}^\dagger = \gamma_{1,2}$  and the anti-commutation relations of the Clifford algebra,  $\{\gamma_i, \gamma_j\} = 2\delta_{ij}$ . The energy  $\xi$  characterizes the degree of the overlap of the MZMs. Small values of  $\xi$  correspond to situations when the two Majoranas are well separated while for large values of  $\xi$  the two MZMs merge into a single Dirac fermion.

The tunneling between the QD and contacts as well as between the QD and TS may be taken into account via, respectively, the Hamiltonians  $\hat{H}_{d-c} = \sum_{l=L,R} \sum_k (\mathcal{T} c_{lk}^\dagger d + \mathcal{T}^* d^\dagger c_{lk})$  and  $\hat{H}_{d-tsc} = \gamma_1(\eta d - \eta^* d^\dagger)$ . The intensities of the tunneling mechanisms  $\hat{H}_{d-c}$  and  $\hat{H}_{d-tsc}$  are characterized by the energies  $\Gamma = 2\pi\nu_c|\mathcal{T}|^2$  and  $|\eta|$ , respectively.

The quantum noise of the nonequilibrium thermoelectric current may conveniently be obtained using the

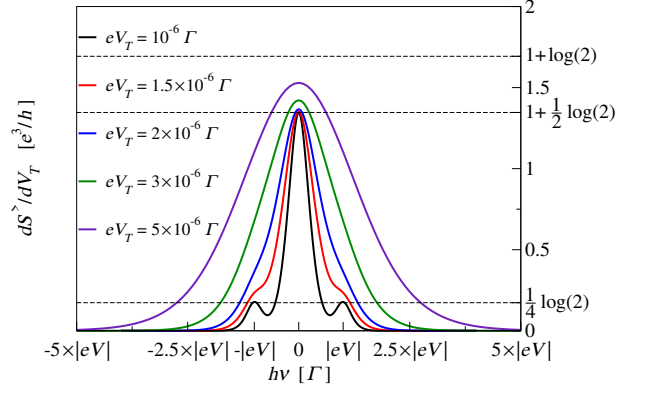


FIG. 3. DTQN  $\partial S^>(\nu, V, V_T)/\partial V_T$  as a function of the frequency  $\nu$  is shown in the regimes  $eV_T < |eV|$ :  $eV_T = 0.5|eV|$  (purple),  $eV_T = 0.3|eV|$  (green),  $eV_T = 0.2|eV|$  (blue) and  $eV_T \ll |eV|$ :  $eV_T = 0.15|eV|$  (red),  $eV_T = 0.1|eV|$  (black). The other parameters have the same values as in Fig. 2.

Keldysh generating functional [32],

$$Z[J_l(t)] = \int \mathcal{D}[\bar{\theta}(t), \theta(t)] e^{\frac{i}{\hbar} S_K[\bar{\theta}(t), \theta(t); J_l(t)]}, \quad (1)$$

$$\{\theta(t)\} = \{\psi(t), \phi_{lk}(t), \zeta(t)\},$$

with the Grassmann fields of the QD,  $\psi(t)$ , contacts,  $\phi_{lk}(t)$ , and TS,  $\zeta(t)$ , defined on the Keldysh closed time contour,  $t \in \mathcal{C}_K$ . In particular, to analyze correlations between the values  $I_l(t)$  and  $I_{l'}(t')$  of the thermoelectric current at different instants of time,  $t$  and  $t'$ , one may introduce the source fields  $J_{lq}(t)$  (subscript  $q$  denotes the forward/backward branch of  $\mathcal{C}_K$ ,  $q = \pm$ ),

$$S_{scr} = - \int_{-\infty}^{\infty} dt \sum_{l=L,R} \sum_{q=+,-} J_{lq}(t) I_{lq}(t), \quad (2)$$

$$I_{lq}(t) = \frac{ie}{\hbar} \sum_k [\mathcal{T} \bar{\phi}_{lkq}(t) \psi_q(t) - \mathcal{T}^* \bar{\psi}_q(t) \phi_{lkq}(t)],$$

$$\langle I_l(t) I_{l'}(t') \rangle = (i\hbar)^2 \frac{\delta^2 Z[J_l(t)]}{\delta J_{l-}(t) \delta J_{l'+}(t')} \Big|_{J_{lq}(t)=0}. \quad (3)$$

We focus on the greater noise correlation function in the left contact,  $S^>(t-t'; V, V_T) = \langle I_L(t) I_L(t') \rangle - I_L^2(V, V_T)$ , where  $I_L(V, V_T)$  is the mean thermoelectric current. Due to the stationary conditions it depends only on the difference,  $(t-t')$ , of the instants of time and thus its Fourier transform depends on only one frequency  $\omega$  (or  $\nu$ ,  $h\nu = \hbar\omega$ ). One then obtains the photon emission/absorption spectra,

$$S^{em/ab}(\nu, V, V_T) = \begin{cases} S^>(\nu, V, V_T), & \nu < 0 \\ S^>(\nu, V, V_T), & \nu > 0 \end{cases}, \quad (4)$$

characterizing the thermoelectric transport.

Below our results reveal universality of Majorana thermoelectric quantum fluctuations at finite frequencies via

numerical computations of the DTQN having universal units of  $e^3/h$ . We assume the strong Majorana tunneling regime characterized by large values of  $|\eta|$ , that is

$$|\eta| \geq \max\{|\epsilon_d|, |eV|, eV_T, k_B T, \xi\}. \quad (5)$$

Finally, to avoid any misconception, it is important to keep in mind that we explore the quantum noise (see also Refs. [33, 34]). One should not mix it up with the classical shot noise having different physical nature. The latter is given as the symmetrized current-current correlator. As a result, the classical shot noise has symmetric spectra and any discussion of its spectral asymmetry would obviously make no sense.

### III. RESULTS FOR THE MAJORANA THERMOELECTRIC QUANTUM NOISE

First, we show results in the regime  $eV_T \gg |eV|$ . In this regime there appears a resonance around  $\nu = 0$  shown by the solid curves in Fig. 2. The maximum of this resonance is reached at  $\nu = 0$  and takes the universal nontrivial value  $\partial S^>(\nu = 0, V, V_T)/\partial V_T = [1 + \log(2)](e^3/h)$ . In the regime  $|eV| \ll eV_T$  this maximum does not depend on  $\epsilon_d$ ,  $V$  and  $V_T$ . The full width of this resonance at half of its maximum is proportional to  $eV_T$ . Moreover, the resonance demonstrates the full symmetry between the photon emission ( $\nu < 0$ ) and photon absorption ( $\nu > 0$ ) spectra, *i.e.*  $\partial S^>(-\nu, V, V_T)/\partial V_T = \partial S^>(\nu, V, V_T)/\partial V_T$ . In contrast, for the trivial QD system having no TS,  $\xi = 0$ ,  $\eta = 0$ , the spectra, shown by the dashed curves, are not universal since they depend on  $\epsilon_d$ .

When  $eV_T$  becomes comparable and below  $|eV|$ , the resonance shown in Fig. 2 starts to change. This is shown in Fig. 3 for various values of  $eV_T$ , from  $eV_T < |eV|$  down to  $eV_T \ll |eV|$ . The resonance persists in all the curves having the spectral symmetry,  $\partial S^>(-\nu, V, V_T)/\partial V_T = \partial S^>(\nu, V, V_T)/\partial V_T$ . The maximum of the resonance is at  $\nu = 0$  for all the curves. For  $eV_T < |eV|$  the maximum is not universal: it decreases from the universal nontrivial value  $[1 + \log(2)](e^3/h)$ , reached in the regime  $eV_T \gg |eV|$  (see Fig. 2), down to the universal nontrivial value  $[1 + \log(2^{1/2})](e^3/h)$ , reached in the regime  $eV_T \ll |eV|$ . Moreover, when  $eV_T$  becomes much below  $|eV|$ , in the vicinity of  $h\nu = \mp|eV|$  there develop two shoulders (red curve,  $eV_T = 0.15|eV|$ ). If  $eV_T$  is decreased still further, the shoulders turn into nonequilibrium resonances located around  $h\nu = \mp|eV|$  (black curve,  $eV_T = 0.1|eV|$ ). For  $eV_T \ll |eV|$  the maxima of these resonances are at  $h\nu = \mp|eV|$  and take the universal nontrivial value  $[\log(2^{1/4})](e^3/h)$ . As shown in Fig. 4 by solid curves, the full widths of the resonances, located around  $h\nu = 0$  and  $h\nu = |eV|$ , at half of their maxima are proportional to  $eV_T$ . The universality of the maxima  $[1 + \log(2^{1/2})](e^3/h)$  and  $[\log(2^{1/4})](e^3/h)$ , located, respectively, at exactly  $h\nu = 0$  (upper panel) and  $h\nu = |eV|$  (lower panel), manifests in their independence of  $\epsilon_d$ ,  $V$  and  $V_T$ . As the temperature is increased,

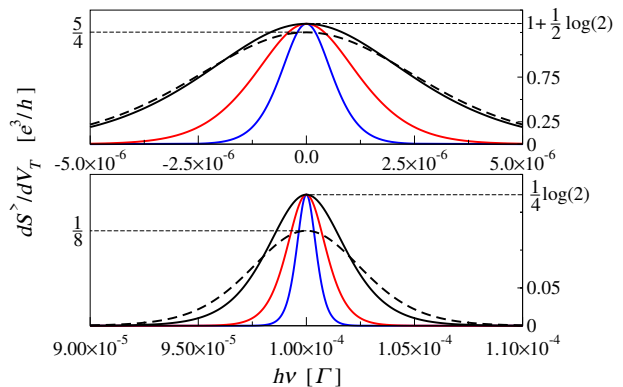


FIG. 4. The resonances of DTQN,  $\partial S^>(\nu, V, V_T)/\partial V_T$ , located around  $h\nu = 0$  (upper panel) and  $h\nu = |eV|$  (lower panel), are shown as functions of the frequency  $\nu$  when  $|eV|$  essentially exceeds  $eV_T$ . Here  $|eV|/\Gamma = 10^{-4}$  while  $eV_T = 10^{-2}|eV|$  (black curves),  $eV_T = 5 \cdot 10^{-3}|eV|$  (red curves) and  $eV_T = 2.5 \cdot 10^{-3}|eV|$  (blue curves). The dashed curves show the universal results for higher temperatures, in the regime  $eV_T \ll k_B T \ll |eV|$ , with  $eV_T = 10^{-4}|eV|$ ,  $k_B T = 10^{-2}|eV|$ . The other parameters have the same values as in Fig. 2.

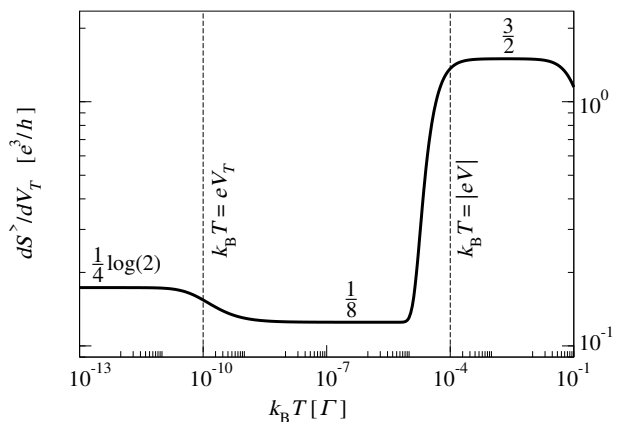


FIG. 5. The universal temperature dependence of DTQN,  $\partial S^>(\nu, V, V_T)/\partial V_T$ , at  $h\nu = |eV|$ . Here  $|eV|/\Gamma = 10^{-4}$  while  $eV_T = 10^{-6}|eV|$ . The other parameters have the same values as in Fig. 2.

the universal spectral symmetry persists and one crosses over through two new regimes,  $eV_T \ll k_B T \ll |eV|$  and  $eV_T \ll |eV| \ll k_B T$ . When  $eV_T \ll k_B T \ll |eV|$ , the resonances located around  $h\nu = 0$  and  $h\nu = \mp|eV|$  persist but, as it is shown by the dashed lines in Fig. 4, their maxima acquire new universal values,  $5e^3/4h$  and  $e^3/8h$ , respectively, and the full widths of the resonances at half of their maxima are proportional to  $k_B T$ . If the temperature is increased still further, the resonances at  $h\nu = 0$  and  $h\nu = \mp|eV|$  widen and finally merge into a single resonance located around  $h\nu = 0$ . The full width of this resonance at half of its maximum is proportional to  $k_B T$ . When  $eV_T \ll |eV| \ll k_B T$ , the maximum of this resonance is exactly at  $h\nu = 0$  and takes the universal value  $3e^3/2h$ . In this regime DTQN at  $h\nu = \mp|eV|$  with

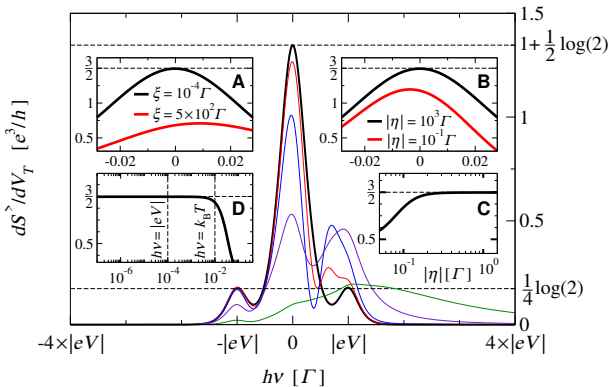


FIG. 6. DTQN  $\partial S^>(\nu, V, V_T)/\partial V_T$  as a function of the frequency  $\nu$  is shown for  $eV_T = 0.1|eV|$ . Here  $\xi/\Gamma = 10^{-4}$  (black),  $\xi/\Gamma = 0.1$  (red),  $\xi/\Gamma = 0.2$  (blue),  $\xi/\Gamma = 0.4$  (purple),  $\xi/\Gamma = 0.8$  (green). The other parameters have the same values as in Fig. 2. Inset A:  $\partial S^>(\nu, V, V_T)/\partial V_T$  for two values of  $\xi$  in the regime  $eV_T \ll |eV| \ll k_B T$  with  $eV_T = 10^{-6}|eV|$ ,  $k_B T = 10^2|eV|$ ,  $|eV|/\Gamma = 10^{-4}$  and  $|\eta|/\Gamma = 10^3$ . Inset B: the same as in Inset A but for two values of  $|\eta|$  and  $\xi/\Gamma = 10^{-4}$ . Inset C:  $\partial S^>(\nu, V, V_T)/\partial V_T$  at  $h\nu = |eV|$  as a function of  $|\eta|$  with other parameters as in Inset B. Inset D: the same as in Inset A but with  $|\eta| = \Gamma$ ,  $\xi/\Gamma = 10^{-4}$ .

very high precision is equal to its value at  $h\nu = 0$ , *i.e.* to  $3e^3/2h$ . DTQN at  $h\nu = |eV|$  is shown in Fig. 5 as a universal function of the temperature over the three regimes  $k_B T \ll eV_T \ll |eV|$ ,  $eV_T \ll k_B T \ll |eV|$  and  $eV_T \ll |eV| \ll k_B T$ .

Let us look at what happens with the above universal spectral symmetry and resonant structure when MZMs significantly overlap or when the coupling strength to the TS is varied. The overlap of MZMs is achieved via increasing  $\xi$ . Note that our model with large values of  $\xi$  may also be interpreted as the one where the QD is coupled to a partially separated Andreev bound state [35] localized near the corresponding end of the TS (see also Ref. [36]). We assume that the Majoranas, composing the partially separated Andreev bound state, significantly overlap but are still well separated in order to neglect the coupling of the second Majorana,  $\gamma_2$ , to the QD. A more general situation with finite couplings of  $\gamma_1$  and  $\gamma_2$  to the QD (see, *e.g.*, Ref. [37]) will be explored in our future research. We also note that, although our model relying upon energy spectra is quite realistic, in experiments it may become necessary to introduce a measure for spatial separation of the two Majoranas [38].

Fig. 6 presents results for  $eV_T = 0.1|eV|$  when the triple resonant structure is present for extremely well ( $\xi/\Gamma = 10^{-4}$ ) separated MZMs. The thin curves illustrate how this perfectly symmetric structure (thick

black curve) gains asymmetry when  $\xi$  increases and the two Majoranas compose a partially separated Andreev bound state. Insets A-D show results in the regime  $eV_T \ll |eV| \ll k_B T$ . In the insets we specify  $\epsilon_d = 0.5\Gamma$ . Inset A shows that also at high temperatures the perfect Majorana spectral symmetry, demonstrated by the black curve, is broken by partially separated Andreev bound states, modeled via large values of  $\xi$ , as demonstrated by the red curve. The black curve in Inset B is a universal (independent of  $\epsilon_d$ ) result demonstrating the Majorana spectral symmetry when Inequality (5) is satisfied. For the red curve in Inset B Inequality (5) is not satisfied and this non-universal (dependent on  $\epsilon_d$ ) curve is asymmetric. The universality (independence of  $\epsilon_d$ ) persists down to  $|\eta| \approx 0.3\Gamma$  as demonstrated in Inset C where DTQN at  $h\nu = |eV|$  is shown as a function of  $|\eta|$ . This function significantly deviates from  $3e^3/2h$  for  $|\eta| < 0.3\Gamma$ . As to the frequency dependence, one may observe the universal plateau  $3e^3/2h$  at  $h\nu \lesssim k_B T$ , as shown in Inset D.

#### IV. CONCLUSION

In conclusion, advantages in experimental testing of our results are obvious. First, it is convenience in observing the universal spectral symmetry which does not require measuring any specific value: the spectral symmetry is either present or not and one immediately distinguishes between Majoranas and other states like partially separated Andreev bound states. Second, at high temperatures,  $eV_T \ll |eV| \ll k_B T$ , one measures the universal value  $3e^3/2h$  at realistic parameters. Indeed, as shown above, the universality is reached when  $|\epsilon_d| \leq |\eta|$  and  $|\eta| \gtrsim 0.3\Gamma$ , *e.g.*  $|\eta| = \Gamma$ , as may be tuned by the corresponding gate voltages. The universal value  $3e^3/2h$  may be observed at  $k_B T/\Gamma = 10^{-2}$ , as in Inset D of Fig. 6. The largest energy scale is then  $\Gamma$ . It must be below the induced superconducting gap  $\Delta$ :  $\Gamma \lesssim \Delta$  or  $k_B T \lesssim 10^{-2}\Delta$ . Refs. [12, 14] give  $\Delta \approx 250$  or  $200 \mu\text{eV}$ . Thus  $T \lesssim 2.5 \mu\text{eV}/k_B \approx 0.03 \text{ K} = 30 \text{ mK}$ . Temperatures below 30 mK are well achievable in modern labs. Since quantum noise detectors have already been proposed [39–41], our results are of direct interest for contemporary experiments detecting in the quantum limit the universal spectral symmetry and resonant structure of DTQN in Majorana mesoscopic setups.

#### ACKNOWLEDGMENTS

The author thanks Milena Grifoni, Andreas K. Hüttel and Wataru Izumida for useful discussions.

[1] E. Majorana, “Teoria simmetrica dell’elettrone e del positrone,” *Nuovo Cimento* **14**, 171 (1937).

[2] J. Alicea, “New directions in the pursuit of Majorana fermions in solid state systems,” *Rep. Prog. Phys.* **75**,

- 076501 (2012).
- [3] M. Leijnse and K. Flensberg, “Introduction to topological superconductivity and Majorana fermions,” *Semicond. Sci. Technol.* **27**, 124003 (2012).
- [4] M. Sato and S. Fujimoto, “Majorana fermions and topology in superconductors,” *J. Phys. Soc. Japan* **85**, 072001 (2016).
- [5] R. Aguado, “Majorana quasiparticles in condensed matter,” *La Rivista del Nuovo Cimento* **40**, 523 (2017).
- [6] R. M. Lutchyn, E. P. A. M. Bakkers, L. P. Kouwenhoven, P. Krogstrup, C. M. Marcus, and Y. Oreg, “Majorana zero modes in superconductor-semiconductor heterostructures,” *Nat. Rev. Mater.* **3**, 52 (2018).
- [7] A. Yu. Kitaev, “Unpaired Majorana fermions in quantum wires,” *Phys.-Usp.* **44**, 131 (2001).
- [8] L. Fu and C. L. Kane, “Superconducting proximity effect and Majorana fermions at the surface of a topological insulator,” *Phys. Rev. Lett.* **100**, 096407 (2008).
- [9] L. Fu and C. L. Kane, “Josephson current and noise at a superconductor/quantum-spin-Hall-insulator/superconductor junction,” *Phys. Rev. B* **79**, 161408(R) (2009).
- [10] R. M. Lutchyn, J. D. Sau, and S. Das Sarma, “Majorana fermions and a topological phase transition in semiconductor-superconductor heterostructures,” *Phys. Rev. Lett.* **105**, 077001 (2010).
- [11] Y. Oreg, G. Refael, and F. von Oppen, “Helical liquids and Majorana bound states in quantum wires,” *Phys. Rev. Lett.* **105**, 177002 (2010).
- [12] V. Mourik, K. Zuo, S. M. Frolov, S. R. Plissard, E. P. A. M. Bakkers, and L. P. Kouwenhoven, “Signatures of Majorana fermions in hybrid superconductor-semiconductor nanowire devices,” *Science* **336**, 1003 (2012).
- [13] S. M. Albrecht, A. P. Higginbotham, M. Madsen, F. Kuemmeth, T. S. Jespersen, J. Nygård, P. Krogstrup, and C. M. Marcus, “Exponential protection of zero modes in Majorana islands,” *Nature* **531**, 206 (2016).
- [14] H. Zhang, C.-X. Liu, S. Gazibegovic, D. Xu, J. A. Logan, G. Wang, N. van Loo, J. D. S. Bommer, M. W. A. de Moor, D. Car, R. L. M. O. het Veld, P. J. van Veldhoven, S. Koelling, M. A. Verheijen, M. Pendharkar, D. J. Pennachio, B. Shojaei, J. S. Lee, C. J. Palmström, E. P. A. M. Bakkers, S. D. Sarma, and L. P. Kouwenhoven, “Quantized Majorana conductance,” *Nature* **556**, 74 (2018).
- [15] N. Hartman, C. Olsen, S. Lüscher, M. Samani, S. Fallahi, G. C. Gardner, M. Manfra, and J. Folk, “Direct entropy measurement in a mesoscopic quantum system,” *Nature Physics* **14**, 1083 (2018).
- [16] Y. Kleeorin, H. Thierschmann, H. Buhmann, A. Georges, L. W. Molenkamp, and Y. Meir, “Measuring the entropy of a mesoscopic system via thermoelectric transport,” *arXiv:1904.08948* (2019).
- [17] E. Sela, Y. Oreg, S. Plugge, N. Hartman, S. Lüscher, and J. Folk, “Detecting the universal fractional entropy of Majorana zero modes,” *Phys. Rev. Lett.* **123**, 147702 (2019).
- [18] S. Smirnov, “Majorana tunneling entropy,” *Phys. Rev. B* **92**, 195312 (2015).
- [19] A. Yu. Kitaev, “Fault-tolerant quantum computation by anyons,” *Ann. Phys.* **303**, 2 (2003).
- [20] C. Nayak, S. H. Simon, A. Stern, M. Freedman, and S. Das Sarma, “Non-abelian anyons and topological quantum computation,” *Rev. Mod. Phys.* **80**, 1083 (2008).
- [21] F. L. Pedrocchi and D. P. DiVincenzo, “Majorana braiding with thermal noise,” *Phys. Rev. Lett.* **115**, 120402 (2015).
- [22] D. E. Liu, M. Cheng, and R. M. Lutchyn, “Probing Majorana physics in quantum-dot shot-noise experiments,” *Phys. Rev. B* **91**, 081405(R) (2015).
- [23] D. E. Liu, A. Levchenko, and R. M. Lutchyn, “Majorana zero modes choose Euler numbers as revealed by full counting statistics,” *Phys. Rev. B* **92**, 205422 (2015).
- [24] C. W. J. Beenakker, “Random-matrix theory of Majorana fermions and topological superconductors,” *Rev. Mod. Phys.* **87**, 1037 (2015).
- [25] A. Haim, E. Berg, F. von Oppen, and Y. Oreg, “Current correlations in a Majorana beam splitter,” *Phys. Rev. B* **92**, 245112 (2015).
- [26] S. Smirnov, “Non-equilibrium Majorana fluctuations,” *New J. Phys.* **19**, 063020 (2017).
- [27] S. Valentini, M. Governale, R. Fazio, and F. Taddei, “Finite-frequency noise in a topological superconducting wire,” *Physica E* **75**, 15 (2016).
- [28] D. Bathellier, L. Raymond, T. Jonckheere, J. Rech, A. Zazunov, and T. Martin, “Finite frequency noise in a normal metal - topological superconductor junction,” *Phys. Rev. B* **99**, 104502 (2019).
- [29] S. Smirnov, “Majorana finite-frequency nonequilibrium quantum noise,” *Phys. Rev. B* **99**, 165427 (2019).
- [30] S. Smirnov, “Universal Majorana thermoelectric noise,” *Phys. Rev. B* **97**, 165434 (2018).
- [31] A. A. Clerk, M. H. Devoret, S. M. Girvin, F. Marquardt, and R. J. Schoelkopf, “Introduction to quantum noise, measurement, and amplification,” *Rev. Mod. Phys.* **82**, 1155 (2010).
- [32] A. Altland and B. Simons, *Condensed Matter Field Theory*, 2nd ed. (Cambridge University Press, Cambridge, 2010).
- [33] G. B. Lesovik and R. Loosen, “On the detection of finite-frequency current fluctuations,” *JETP Lett.* **65**, 295 (1997).
- [34] U. Gavish, Y. Levinson, and Y. Imry, “Detection of quantum noise,” *Phys. Rev. B* **62**, R10637(R) (2000).
- [35] C. Moore, T. D. Stanescu, and S. Tewari, “Two-terminal charge tunneling: Disentangling Majorana zero modes from partially separated Andreev bound states in semiconductor-superconductor heterostructures,” *Phys. Rev. B* **97**, 165302 (2018).
- [36] M. Hell, K. Flensberg, and M. Leijnse, “Distinguishing Majorana bound states from localized Andreev bound states by interferometry,” *Phys. Rev. B* **97**, 161401(R) (2018).
- [37] D. J. Clarke, “Experimentally accessible topological quality factor for wires with zero energy modes,” *Phys. Rev. B* **96**, 201109(R) (2017).
- [38] M.-T. Deng, S. Vaitiekėnas, E. Prada, P. San-Jose, J. Nygård, P. Krogstrup, R. Aguado, and C. M. Marcus, “Nonlocality of Majorana modes in hybrid nanowires,” *Phys. Rev. B* **98**, 085125 (2018).
- [39] D. V. Averin, “Quantum computing and quantum measurement with mesoscopic Josephson junctions,” *Fortschr. Phys.* **48**, 1055 (2000).
- [40] A. A. Clerk and A. D. Stone, “Noise and measurement efficiency of a partially coherent mesoscopic detector,” *Phys. Rev. B* **69**, 245303 (2004).

- [41] D. Mozyrsky, I. Martin, and M. B. Hastings, “Quantum-limited sensitivity of single-electron-transistor-based displacement detectors,” *Phys. Rev. Lett.* **92**, 018303 (2004).